

Full length article

Influence of ruthenium on microstructural evolution in a model Co–Al–W superalloy

Daniel J. Sauza^a, Peter J. Bocchini^a, David C. Dunand^{a, *}, David N. Seidman^{b, **}^a Northwestern University, Department of Materials Science & Engineering, 2220 Campus Drive, Evanston IL 60208, USA^b Northwestern University Center for Atom-Probe Tomography (NUCAPT), 2220 Campus Drive, Evanston IL 60208, USA

ARTICLE INFO

Article history:

Received 4 May 2016

Received in revised form

4 July 2016

Accepted 4 July 2016

Available online 16 July 2016

Keywords:

Cobalt-base superalloys

Microstructure

Atom probe tomography (APT)

Coarsening kinetics

ABSTRACT

The effect of 2 at.% Ru addition on the elemental partitioning and microstructural evolution of a base Co-8.8Al-7.3W at.% superalloy, consisting of a γ -(fcc) matrix with γ' -(L1₂ structure) precipitates is studied using scanning electron microscopy and atom-probe tomography. Ruthenium partitions to the γ' -precipitates in the Co-9.4Al-7.5W-2.1Ru at.% alloy with a partitioning coefficient, $K_{\text{Ru}}^{\gamma'/\gamma} = 1.27$, after aging at 900 °C for 16 h, in contrast to the behavior observed in Ni-base superalloys and theoretically predicted for Co-base superalloys, for which Ru partitions preferentially to the γ -phase. The addition of ruthenium does not significantly affect the γ' volume-fraction or the coarsening kinetics of the γ' precipitates compared to the base ternary alloy. The addition of Ru also leads, however, to a rapid discontinuous transformation of (γ plus γ'), which initiates at the grain boundaries after 128 h aging at 900 °C; (γ plus γ') is transformed into a lamellar phase mixture containing Co₃W (D0₁₉), fcc solid-solution (γ), and Co(Al,W) (B2). After 256 h aging at 900 °C in the Ru-containing alloy, some grains have completely transformed, although regions of γ plus γ' persist. The base ternary Co–Al–W alloy does not exhibit a discontinuous transformation and contains a (γ plus γ') microstructure up to 1024 h of aging at 900 °C.

© 2016 Acta Materialia Inc. Published by Elsevier Ltd. All rights reserved.

1. Introduction

The relatively recently discovered γ' (L1₂ structure)-strengthened Co-base superalloys, based on the Co–Al–W system [1], have generated a great deal of interest for the potential of these alloys to surpass the high-temperature performance of Ni-base superalloys, which contain 10–12 alloying elements and are capable of operating to 1150 °C [2]. The ternary Co–Al–W system suffers, however, from a low γ' -solvus temperature relative to those of commercial Ni-base superalloys [3,4] and the two-phase (γ plus γ') field is generally thought to be metastable at elevated temperatures [5,6]. Recent efforts have focused on stabilizing the (γ plus γ') microstructure and increasing the γ' -solvus temperature by adding strong γ' -forming elements such as Ti and Ta [7–12], which possess among the highest partitioning coefficients reported for quaternary and quinary Co–Al–W-based systems. The partitioning coefficient, $K_i^{\gamma'/\gamma}$, is defined herein as the ratio of the concentration

of an element i in the γ' -precipitate phase to its concentration in the γ -matrix. Higher values of $K_i^{\gamma'/\gamma}$, typically above 2, are correlated with large negative free energies of formation of Co₃X (L1₂) [13]. Partitioning behavior and volume fraction are not, however, the sole indicators of microstructural stability. The addition of 10–20 at.% Ni to ternary Co–Al–W expands the (γ plus γ') phase-field [14], thereby stabilizing the (γ plus γ') phase-field considerably, despite modest increases in the γ' volume-fraction (ϕ) and solvus temperature, and weak partitioning of Ni to γ' [13,15]. A fully-optimized commercial Co-base superalloy will contain a number of refractory alloying elements working in concert to promote improved high-temperature performance, necessitating a firm understanding of the behavior of each potential alloying element. The main objective of this article is to determine experimentally the effects of Ru additions on the partitioning behavior and microstructure of γ' -strengthened Co-base superalloys.

In Ni-base superalloys, Ru has been investigated as a less-costly replacement for Re, and has been shown to partition preferentially to the γ -phase, with $K_{\text{Ru}}^{\gamma'/\gamma}$ ranging from 0.2 to 0.6 [16–21]. There is evidence that the presence of Ru in the γ -matrix of nickel-based superalloys acts to inhibit the formation of deleterious topologically close-packed (TCP) phases, which form at high temperatures

* Corresponding author.

** Corresponding author.

E-mail addresses: dunand@northwestern.edu (D.C. Dunand), d-seidman@northwestern.edu (D.N. Seidman).

[16,21–28]. To date only four studies mention the effects of Ru in the γ' -strengthened Co-base systems: (i) a first-principles study of site-preference in γ' -Co₃(Al,W) indicates that Ru has a weak preference for the Co-site [29]; (ii) a subsequent study on the substitutional formation energies of Ru and Re on both sides of the γ/γ' interface in Co–Al–W reported that Ru partitions to the γ -matrix with a $K_{Ru}^{\gamma/\gamma'}$ value of about 0.006 at 900 °C; this value was obtained by calculating substitutional formation energies at 0 K for incorporating Ru atoms into model γ - and γ' -configurations on either side of the heterophase interface, which does not include entropic effects [30]. This predicted trend of γ -partitioning is qualitatively comparable to the behavior observed in Ni-base systems containing Ru [16,18,23]. Finally, (iii) experimental differential scanning calorimetry (DSC) measurements demonstrate that the addition of 2 at.% Ru to a Co–9Al–10W alloy reduces the γ' -solvus temperature by 8 K and increases the γ -solidus temperature by 5 K, when compared to the base ternary alloy [13]. If Ru additions in Co-base superalloys promote a similar stabilizing effect as observed in Ni-base alloys, the addition of small concentrations of Ru may inhibit TCP-formation in γ , thereby promoting the stability of (γ plus γ') phase field. The small reduction in the γ' -solvus temperature may be mitigated by Ti and/or Ta additions, which are known to improve significantly the γ' -solvus temperature of these alloys [8,31]. In this article we investigate experimentally, for the first time, the partitioning effect of Ru, as well as its effect on the (γ plus γ') phase-field stability in a Co–8.8Al–7.3W alloy.

2. Experimental procedures

2.1. Alloy preparation and heat treatment

The base Co–8.8Al–7.3W alloy employed was synthesized via induction melting from pure elements. A portion of this ternary base alloy was used to produce an 8 g button with a nominal composition of Co–9.7Al–7.1W–2.1Ru at.% by arc-melting it together with a high-purity Ru powder, enclosed in high-purity Al foil, thereby preventing a loss of Ru during arc-melting. The button was arc-melted five times, flipping after each melting step to ensure thoroughly mixing the alloy. Sections of both the ternary and quaternary alloys were vacuum-encapsulated in quartz ampoules, which are backfilled with argon and subjected to a two-stage heat-treatment to promote chemical homogeneity: (i) homogenization in the γ (fcc) phase-field at 1300 °C for 24 h; (ii) solution treatment at 1150 °C for 4 h followed by a water quench. The specimens were then re-encapsulated and aged at 900 °C followed by water-quenching. Specimens of the Ru-containing alloy were aged for 0, 4, 16, 64, 128, and 256 h, while specimens of the base ternary alloy were aged for 4, 64, 256, and 1024 h.

2.2. Characterization and analysis methods

Characterization of the microstructure and bulk composition of this alloy was performed utilizing a Hitachi SU8030 scanning electron microscope (SEM) equipped with a cold-field-emission source, operating at 10 kV with an 8–10 mm working distance. An as-quenched sample as well as all aged samples were polished mechanically and then chemically-etched at room temperature, using a solution of 33% acetic acid, 33% hydrochloric acid (12.1 M), and 1% hydrofluoric acid by volume in de-ionized water. The bulk Ru-containing alloy composition was measured using energy dispersive spectroscopy (EDS) using the same SEM as noted above, and is Co–9.4Al–7.5W–2.1Ru at. %. Representative electron micrographs used to quantify precipitate morphology were recorded for grains exhibiting a <100>-type orientation perpendicular to the electron-beam's axis; the γ' -precipitates appear as squares or

rectangles in the 2D cross-section. Between 300 and 600 precipitates for each aging condition were hand-traced using NIH ImageJ (version 1.48) and the area A of each γ' -precipitate was used to calculate a circular areal-equivalent radius, $R = \sqrt{A/\pi}$. The γ' -precipitate volume fraction, $\phi^{\gamma'}(t)$, and the areal γ' -precipitate number density, $N_A(t)$, for each aging condition were stereologically determined using the line-intercept method applied directly to SEM micrographs [32]. The precipitate number density per unit volume, $N_V(t)$, was then calculated using the stereological relationship [32]

$$N_V = \frac{N_A}{2 \langle R \rangle} \quad (1)$$

where $\langle R \rangle$ is the mean areal-equivalent radius.

To determine the compositions of the γ' - and γ -phases (and by extension, the partitioning behavior), APT specimens were prepared by cutting aged samples into ~1 cm-long rectangular prisms with a 0.4×0.4 mm² cross-sections [33]. Specimens were electrochemically polished at room temperature using solutions of 20% chromic acid and 30% hydrochloric acid (12.1 M) in de-ionized water for coarse polishing and 2% perchloric acid, 1% chromic acid, and 1% hydrochloric acid in 2-butoxyethanol by volume for fine polishing; electropolishing was performed at 5.5–20 V dc [34]. APT was performed using a LEAP 4000X-Si system employing an ultraviolet (wavelength = 355 nm) picosecond laser with a pulse energy of 20 pJ, a specimen base temperature of 25 ± 1 K, a detection rate of 5%, and a pulse repetition rate of 250 kHz. Data analyses were performed using the IVAS 3.6.6 software package (Cameca, Madison, WI). The γ' -precipitates were identified and studied quantitatively using the proximity histogram [35,36] and envelope methods [37,38].

3. Results and discussion

γ' -precipitates were not observed in the as-solutionized samples and the bulk of these samples appeared homogeneous within the spatial resolution of the SEM-EDS (~1 μ m). Contrast indicative of dendrite cores and interdendritic regions was not observed via SEM in the as-solutionized sample, although some residual microsegregation may be expected. In the base Co–Al–W alloy, a two-phase (γ plus γ') microstructure, with no evidence of other phases, even at GBs, is observed up to 1024 h aging at 900 °C, which is the longest aging time investigated. In the Ru-containing alloy, a (γ plus γ') microstructure is observed after 4, 16, and 64 h of aging at 900 °C. After 128 h of aging the microstructure of the Ru-containing alloy is dominated by colonies consisting of lamellar structures emanating from γ/γ' grain boundaries, which are growing at the expense of the two-phase (γ plus γ') grains; after 256 h of aging many of the (γ plus γ') grains are consumed by this lamellar structure. Despite the appearance of this discontinuous transformation at longer aging times, regions of the (γ plus γ') microstructure persist for all aging conditions investigated, permitting a quantitative analysis of the γ' - morphology. The microstructural evolution of this alloy is discussed as follows: (1) regions containing solely a (γ plus γ') microstructure; and (2) regions consisting of the discontinuously transformed lamellar structure.

3.1. Evolution of (γ plus γ') microstructure

3.1.1. Growth and coarsening of γ' -precipitates within regions exhibiting only a (γ plus γ') microstructure

Fig. 1 displays SEM micrographs of γ' -precipitates (rectangular cross-sections) against a background of chemically-etched γ -

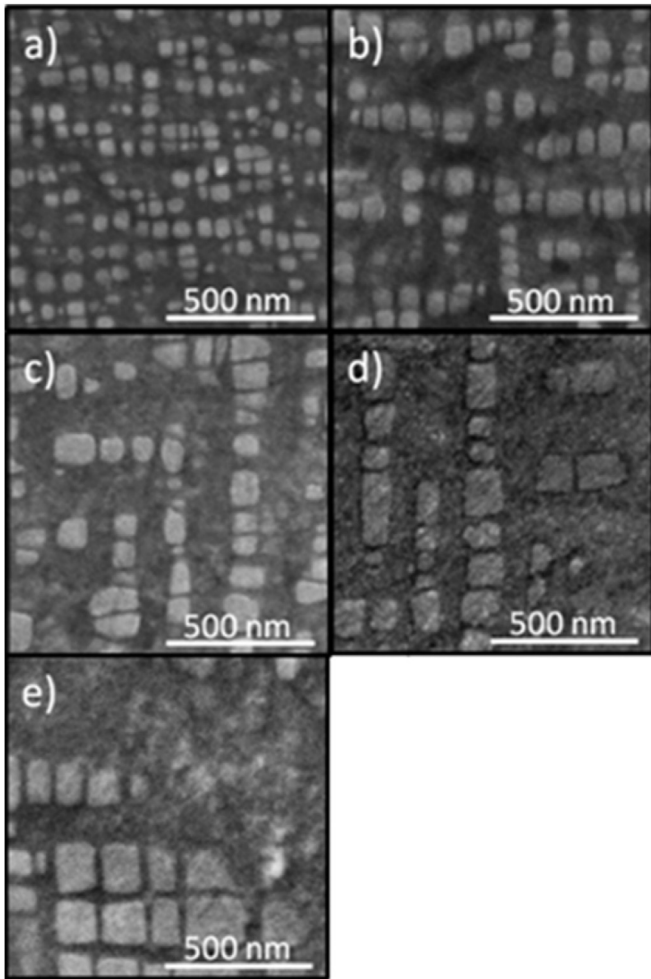


Fig. 1. SEM micrographs of chemically-etched regions of Co-9.4Al-7.5W-2.1Ru at.% containing a two-phase (γ plus γ') microstructure after aging at 900 °C for: (a) 4, (b) 16, (c) 64, (d) 128, and (e) 256 h.

matrix. Micrographs were recorded at a constant magnification of 60 kx and an accelerating voltage of 10 kV for each aging condition. For comparison, Fig. 2 exhibits micrographs of the (γ plus γ') microstructure for the case of the ternary Co–Al–W base alloy. All micrographs are recorded for grains oriented along $\langle 100 \rangle$ -type directions with respect to the surface normal, ensuring that the observed microstructure provides a consistent 2D cross-sectional view of the temporal evolution of the 3D precipitate morphology. After 4 h of aging, the γ' -precipitates are homogeneously distributed throughout the bulk and already exhibit a cuboidal morphology with their alignment occurring along a $\langle 100 \rangle$ -type direction, which is similar to aged and coherent γ' -precipitates in Ni-base superalloys. After 256 h, individual γ' -precipitates exhibit a larger aspect ratio than the near 1:1 square γ' -precipitate cross-sections observed at 4 h of aging, suggesting that a coagulation and coalescence mechanism is occurring among adjacent cuboids, as previously described for an aging study of a model Ni–Al–Cr system compared with Ni–Al–Cr–W [39]. With increasing aging times, several morphological trends are observed: (i) the γ' -precipitates are coarsening, resulting in a continuous increase in the mean radius, $\langle R(t) \rangle$, and concomitantly a continuous decrease in the precipitate number density, N_v , addressed quantitatively below; and (ii) the alignment of cuboidal γ' -precipitates becomes more pronounced, with the γ' -precipitates becoming more densely

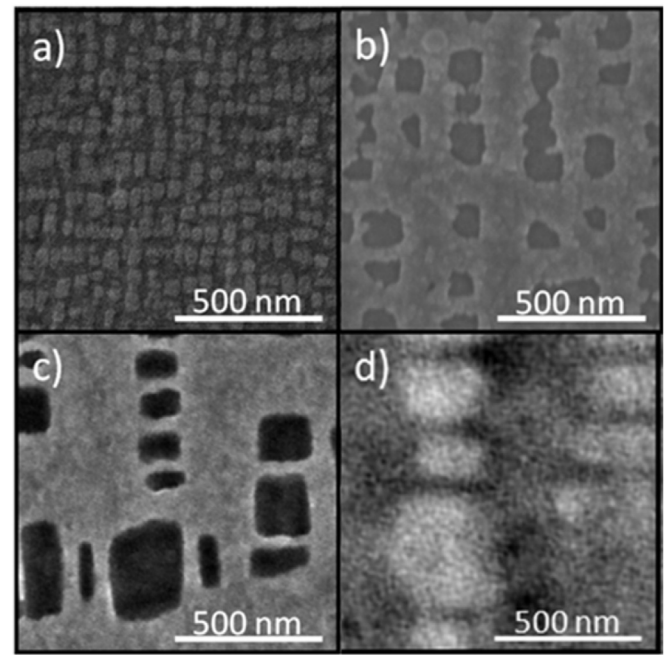


Fig. 2. SEM micrographs of Co-8.8Al-7.3W at.% displaying chemically-etched regions containing a representative two-phase (γ plus γ') microstructure after aging at 900 °C for: (a) 4, (b) 64, (c) 256, and (d) 1024 h.

packed, arranged in long chains oriented along orthogonal $\langle 100 \rangle$ -type directions. The alignment of γ' -precipitates in coarsening alloys is called rafting, which is observed in both unstressed and stressed specimens. Load-free directional coarsening has been previously observed in Ni–Al and Ni–Al–Cr as well as commercial Ni-base superalloys [39–42]. In Ni-base superalloys, strong γ' -precipitate forming elements, such as Al and Ti, tend to occur in the interdendritic regions, while refractory elements, such as W and Ru, tend to be enriched in the dendrite cores [43–45]. As a result, γ' -precipitates form preferentially in inter-dendritic regions, resulting in stresses arising from the lattice parameter mismatch due to the thermal expansion coefficients of the two phases. This dendritic stress is thought to be a primary driving force for load-free directional coarsening [42,46,47]. In the case of Co-base superalloys, W is a strong γ' -precipitate former; it is thus possible that the situation is reversed from the case of Ni-base superalloys, with γ' -precipitates instead forming preferentially in the dendritic cores; this subject is beyond the scope of this article. The γ' -precipitate volume fractions of both the base Co–Al–W and quaternary Co–Al–W–Ru alloys for a given aging time, $\phi^{\gamma'}(t)$, were calculated directly from the SEM micrographs, Fig. 3. At 64 h of aging at 900 °C, the values of $\phi^{\gamma'}(t)$ for Co–Al–W and Co–Al–W–Ru are 24.4 ± 1.8 and $25.2 \pm 1.8\%$, respectively. After 256 h, $\phi^{\gamma'}(t)$ is $24.8 \pm 1.8\%$ for Co–Al–W and $26.6 \pm 1.5\%$ for Co–Al–W–Ru, respectively. The values of $\phi^{\gamma'}(64 \text{ h})$ and $\phi^{\gamma'}(256 \text{ h})$ are the same within error for both Co–Al–W and Co–Al–W–Ru, suggesting that $\phi^{\gamma'}(t)$ is asymptotically approaching its equilibrium value, ϕ^{eq} for both alloys. Additionally, the average value of $\phi^{\gamma'}(t)$ for times greater than 16 h, at 900 °C, is 26.7 ± 2.3 for Co–Al–W and 25.7 ± 1.8 for the Ru-containing alloy, respectively; the values are equivalent within error, suggesting that the addition of 2 at.% Ru to the base alloy does not affect strongly ϕ^{eq} . The larger values of $\phi^{\gamma'}(t)$ observed at 4 h aging: $42.8 \pm 1.5\%$ for Co–Al–W and $29.4 \pm 1.5\%$ for Co–Al–W–Ru, may be due to an artifact caused by over-etching the γ -matrix, resulting in additional exposed planes of γ' -precipitates if the polish-relief depth approaches $\langle R(t) \rangle$. For chemically-etched

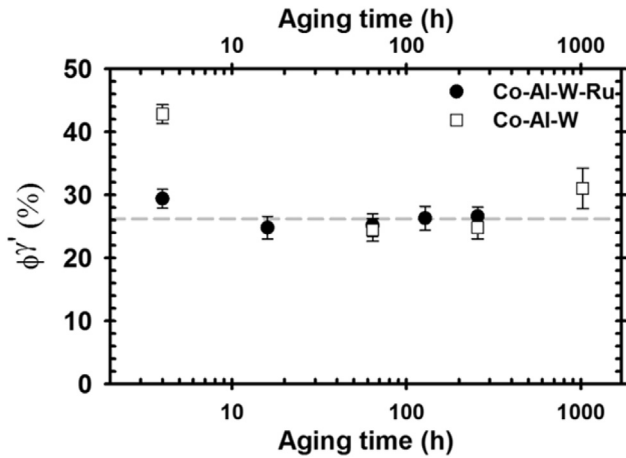


Fig. 3. Volume fraction of γ' for the Ru-containing and ternary alloys plotted against aging time at 900 °C, as determined via SEM micrographs. The dashed line denotes $\phi_{\gamma'}(t) = 26\%$, the mean value starting from 16 h of aging for the Ru-containing sample.

model Ni–Al–Cr and Ni–Al–Cr–W alloys, Sudbrack et al. measured experimentally utilizing atomic force microscopy (AFM) polish-relief depths ranging from several to tens of nm [4], which is on the order of $\langle R(t) \rangle$, for ternary Co–Al–W aged at 900 °C for 4 h, 7.98 ± 7.0 nm. The value of ϕ^{eq} for Co–Al–W–Ru observed in this study, $25.7 \pm 1.8\%$, is small compared to the high volume fractions (50–70%) reported in the literature, which may be due to the smaller tungsten concentrations of 7.3 at.% W for the base ternary alloy and 7.1 at.% for the quaternary alloy [3,48,49]. For each aging condition, $\langle R(t) \rangle$ was calculated from all the measured radii, R . The values of $\langle R(t) \rangle$ are plotted versus aging time, Fig. 4a, for the base-ternary and Ru-containing alloys. For the aging times studied the values of $\langle R(t) \rangle$ of γ' -precipitates in the ternary Co–Al–W and quaternary Co–Al–W–Ru alloy are equivalent within error, although $\langle R(t) \rangle$ measured for the ternary Co–Al–W alloy for a given aging time is consistently larger than $\langle R(t) \rangle$ measured for the Ru-containing alloy, suggesting that diffusion is decelerated by the addition of Ru: $\langle R(t) \rangle$ at 64 h is 49.18 ± 18.6 nm for Co–Al–W and 40.61 ± 13.73 nm for Co–Al–W–Ru; and at 256 h, $\langle R(t) \rangle$ is 81.68 ± 33.6 nm and 63.40 ± 18.98 nm for Co–Al–W and Co–Al–W–Ru, respectively. The data were further analyzed using a nonlinear multivariable regression procedure [50] to solve for the unknown quantities in:

$$\langle R(t) \rangle^p - \langle R(t_0) \rangle^p = K(t - t_0); \quad (2)$$

where t_0 is defined as the aging time at the onset of quasi-stationary coarsening, p is the temporal exponent, and K is the associated rate constant [50]. This method is strongly preferred over simply plotting $\langle R(t) \rangle^3$ versus t because it is free of assumptions about the value of the temporal exponent and the other two quantities. For our analysis we set t_0 equal to 64 h because of the aforementioned observation that by this time the γ' volume-fraction is asymptotically approaching ϕ^{eq} , implying that the system has achieved at least quasi-stationary coarsening as required by the Lifshitz-Slyozov-Wagner (LSW), Kuehmann-Voorhees (KV), and Philippe-Voorhees (PV) models [39,51,52]. The quantity $\langle R(t) \rangle$ is proportional to $t^{0.34 \pm 0.01}$ for the Co-8.8Al-7.3W alloy and $t^{0.31 \pm 0.02}$ for the Ru-containing alloy; the error is obtained from the nonlinear multivariable regression analysis. The values of the temporal exponents calculated for Co–Al–W and Co–Al–W–Ru are, within error, the value $1/3$ predicted for $1/p$ as predicted by the KV model for a ternary alloy [51] and the PV model for a quaternary

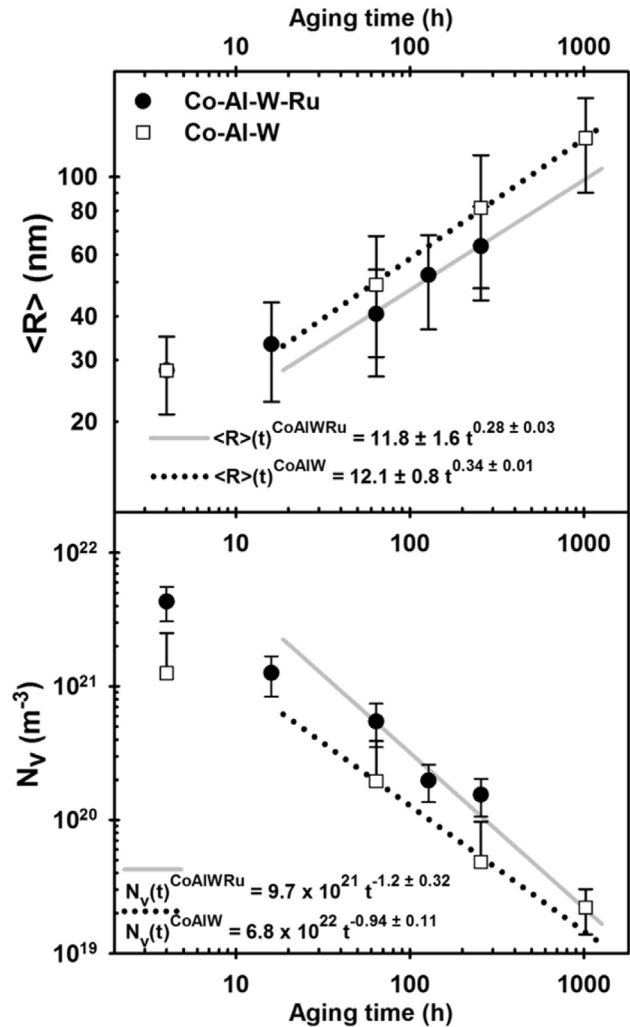


Fig. 4. Temporal evolution of (a) mean radius, $\langle R(t) \rangle$; and (b) number density, $N_V(t)$, of γ' -precipitates measured from within regions containing a two-phase (γ plus γ') microstructure aged at 900 °C for Co-9.4Al-7.5W-2.1Ru at.% and Co-8.8Al-7.3W at.%.

alloy [52], therefore implying that both alloys exhibit diffusion-limited coarsening behavior. The resulting coarsening rate constants K are 5.5×10^{-28} and $2.7 \times 10^{-28} \text{ m}^3\text{s}$. Fig. 4b depicts the temporal evolution of N_V , which decreases as $t^{-0.94 \pm 0.11}$ for the ternary CoAlW alloy and $t^{-1.2 \pm 0.32}$, for the quaternary alloy; the error in the temporal exponent is determined from the nonlinear multivariable regression analysis of the experimental data. The values of N_V calculated for both Co–Al–W and Co–Al–W–Ru are in good agreement with the LSW [53] model's prediction of t^{-1} , and also consistent with the quasi-stationary coarsening equation described by KV for a ternary alloy [51]:

$$N_V(t) \cong \frac{\phi^{\text{eq}}}{4.74K} t^{-1} \quad (3)$$

The PV model for multicomponent alloys also predicts a rate constant of t^{-1} for the temporal evolution of N_V in the quasi-stationary coarsening regime, but the prefactor K is fairly complicated for systems containing four or more elements [52]. Recently, experimental measurements of the interdiffusivity of Al and transition metal solutes, including W and Ru, in f.c.c. cobalt were used to calculate the activation energy, Q , and pre-exponential factor, D_0 [54]. Applying the results of these calculations from the archival

literature to the aging temperature employed in this study, 900 °C, according to the Arrhenius relationship:

$$\bar{D} = D_0 \exp\left(-\frac{Q}{RT}\right) \quad (4)$$

where \bar{D} is the interdiffusion coefficient, R is the ideal gas constant, and T is the absolute temperature, yields \bar{D} values of $(7.40 \pm 9.01) \times 10^{-18} \text{ m}^2\text{s}^{-1}$ for W, $(6.79 \pm 30.2) \times 10^{-18} \text{ m}^2\text{s}^{-1}$ for Ru, and $(1.09 \pm 1.6) \times 10^{-16} \text{ m}^2\text{s}^{-1}$ for Al in f.c.c. cobalt at 900 °C. Notably, the difference in the interdiffusion coefficients for Ru and W is small compared to that of Al, which is larger by more than one order of

magnitude. The small difference between the interdiffusion coefficients of Ru and W in f.c.c. Co may explain partially the observed negligible effect of Ru additions on the coarsening kinetics of γ' -precipitates compared to the base Co–Al–W alloy in the present study. It is important to distinguish between the interdiffusivity of a single solute species in pure f.c.c. cobalt and that of a species in a multicomponent alloy; with three or more elements, because the rate constants are more complicated as they depend on the terms of an $n \times n$ diffusion matrix, where n is the number of species [52]. It has been determined experimentally utilizing APT experiments and lattice kinetic Monte-Carlo (LKMC) simulations for several model Ni–Al–Cr alloys that the off-diagonal terms of the diffusion matrix

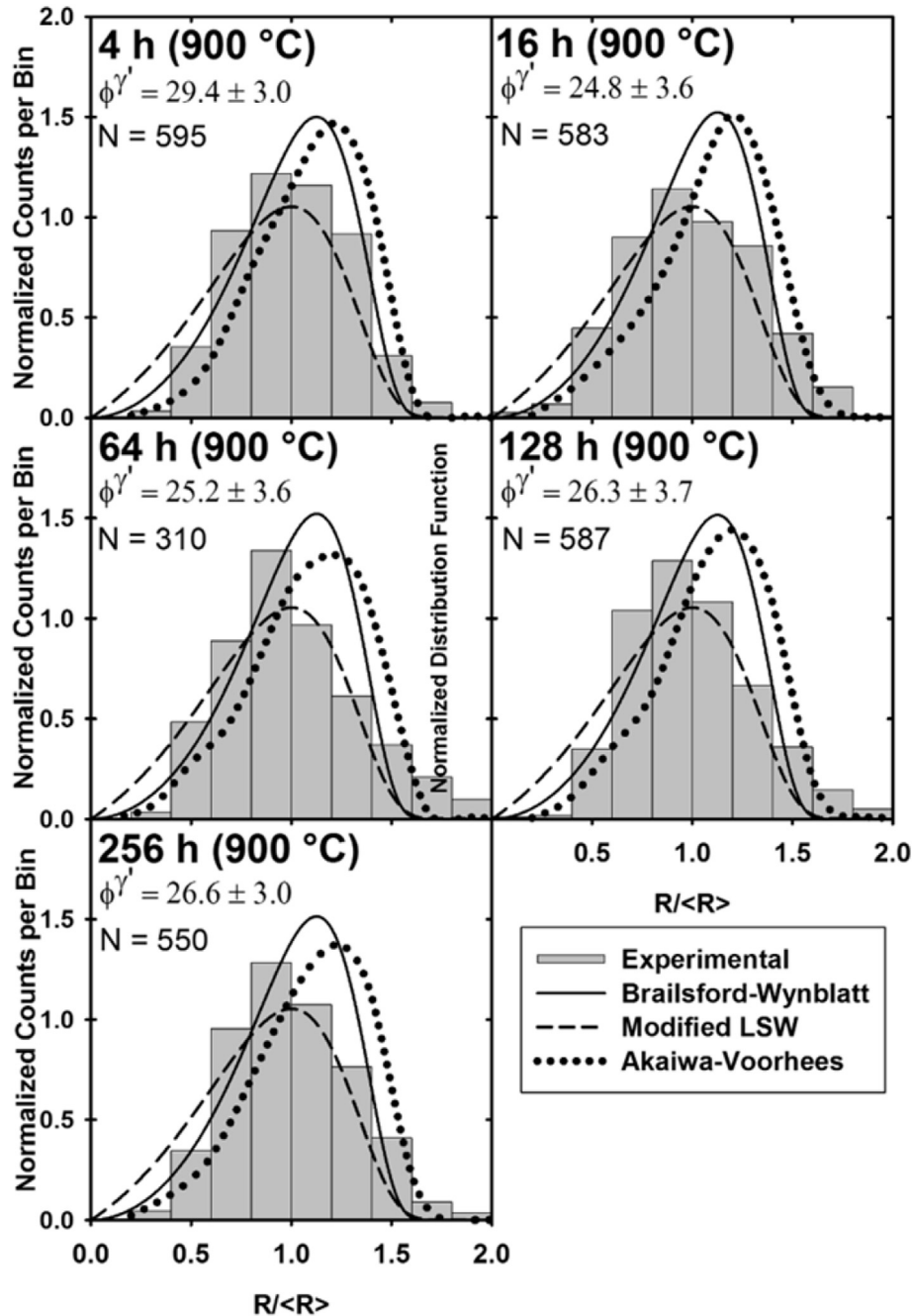


Fig. 5. Temporal evolution of the scaled γ' -precipitate size distributions (PSDs) measured for Co-9.4Al-7.5W-2.1Ru at.% within regions containing a two-phase (γ plus γ') after aging at 900 °C for: (a) 4 h, (b) 16 h, (c) 64 h, (d) 128 h, and (e) 256 h. Line plots represent the stationary-state predictions of Brailsford and Wynblatt [57] (solid line), the modified LSW model [53] (dashed line), and Akaiwa and Voorhees [58] (dotted line) models for the corresponding γ' volume fractions.

carry flux, and thus cannot be disregarded [55]. Hence, the coarsening kinetics of a multicomponent system is not accurately captured by only considering the slowest-diffusing species, as is commonly done, because they involve complex solute-vacancy interactions.

Precipitate size distributions (PSD) were created for each alloy and aging condition by plotting on the abscissa axis the normalized equivalent radius, $R/\langle R(t) \rangle$, and on the ordinate axis the number of γ' -precipitates for a given interval width (20% of the normalized radius) divided by the total precipitate count and the scaled interval width [56]. This method normalizes the area under each histogram to unity, permitting direct comparison among PSDs for different aging times. Experimental PSDs are presented in Figs. 5 and 6 and compared to the predictions of the Brailsford-Wynblatt (BW) [57], the modified LSW [53], and the Akaiwa-Voorhees (AV) models [58], using the experimental values of $\phi^{\gamma'}$ determined for each aging condition. The AV model is utilized to simulate PSDs for all but the ternary specimen aged 4 h at 900 °C, with a measured $\phi^{\gamma'} = 42.8\%$, as this model does not account for precipitate overlap during coarsening, which leads to errors in the simulations for values of $\phi^{\gamma'}$ greater than about 30% [58]. Of the three models investigated, the modified LSW and BW distributions appear visually to provide a better qualitative agreement with the experimental PSDs. The PSDs are evolving continuously with increasing aging time, gradually shifting from a left-skewed to a more right-skewed PSD, suggesting that the PSDs for both alloys have not yet achieved their equilibrium shapes.

3.1.2. Atom-probe tomographic analyses of γ' -precipitates

APT was performed on a specimen aged for 16 h. The resulting 3D reconstruction, Fig. 7a, consists of 9×10^6 atoms and contains three partial γ' -precipitates in a γ -matrix. Proximity histograms demonstrating the partitioning behavior between the γ - and γ' -phases are also displayed. The measured compositions of the γ - and γ' -phases, determined by averaging the concentration values away from the γ/γ' interface, the so-called far-field (*ff*) values, are reported in Table 1. One standard deviation was determined employing counting statistics, which was determined from:

$$\sigma = \sqrt{\frac{C_i(1 - C_i)}{N_T}} \quad (5)$$

where σ is the statistical counting uncertainty, C_i is the measured concentration of species i at a given distance from the interface, and N_T is the total number of type i atoms collected in the sampled region. We find that Co, Al, and W are similar in their behavior to what is reported in the archival literature for other model Co-base systems [10,15,59,60]. Tungsten partitions strongly to γ' -phase precipitates ($K_W^{\gamma'/\gamma} = 2.27 \pm 0.15$), Co partitions to the γ -matrix ($K_{Co}^{\gamma'/\gamma} = 0.89 \pm 0.01$), and Al partitions to γ' -phase precipitates ($K_{Al}^{\gamma'/\gamma} = 1.13 \pm 0.07$). In Co–Al–W–Ru we find that Ru partitions to the γ' phase, $K_{Ru}^{\gamma'/\gamma} = 1.27 \pm 0.18$, in contrast to the behavior predicted via first-principles calculations for a 192 atom Co–Al–W supercell model containing Ru additions [30]. Ruthenium partitioning preferentially to the γ' -phase is also opposite to its behavior

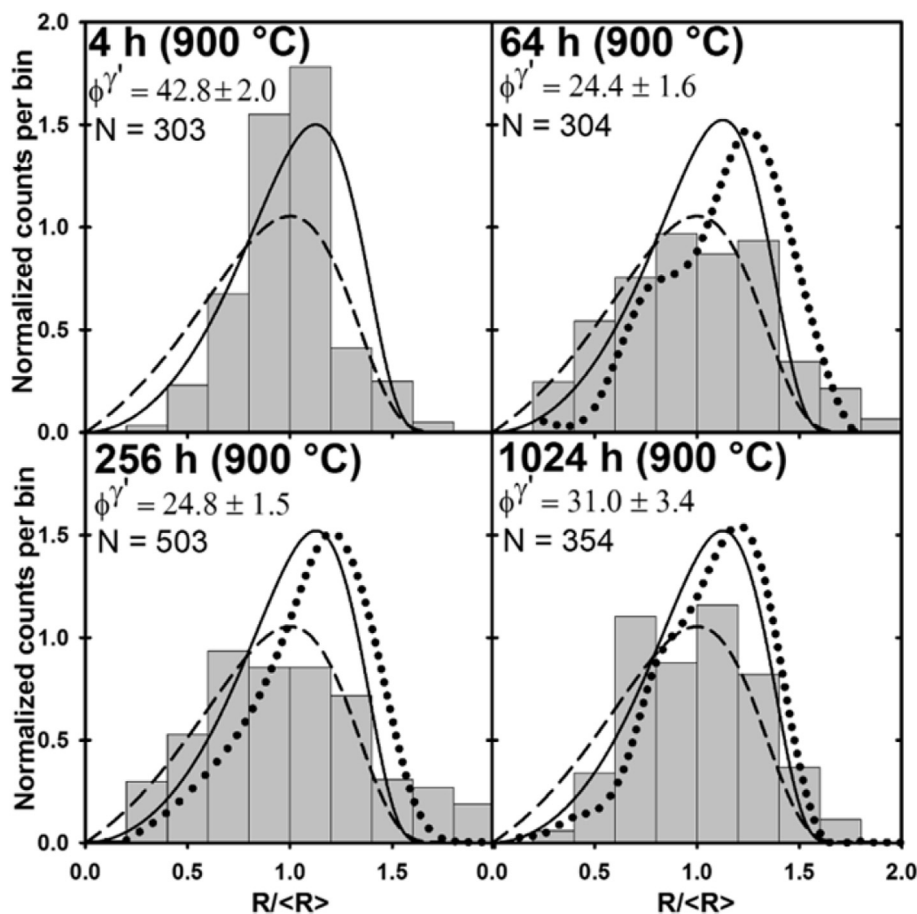


Fig. 6. Temporal evolution of the scaled γ' -precipitate size distributions measured for Co-8.8Al-7.3W at.% after aging at 900 °C for: 4 h, 64 h, 128 h, 1024 h. Line plots represent the stationary-state predictions of Brailsford and Wynblatt [57] (solid line), the modified LSW [53] (dashed line), and Akaiwa and Voorhees [58] (dotted line) models for the corresponding γ' volume fractions.

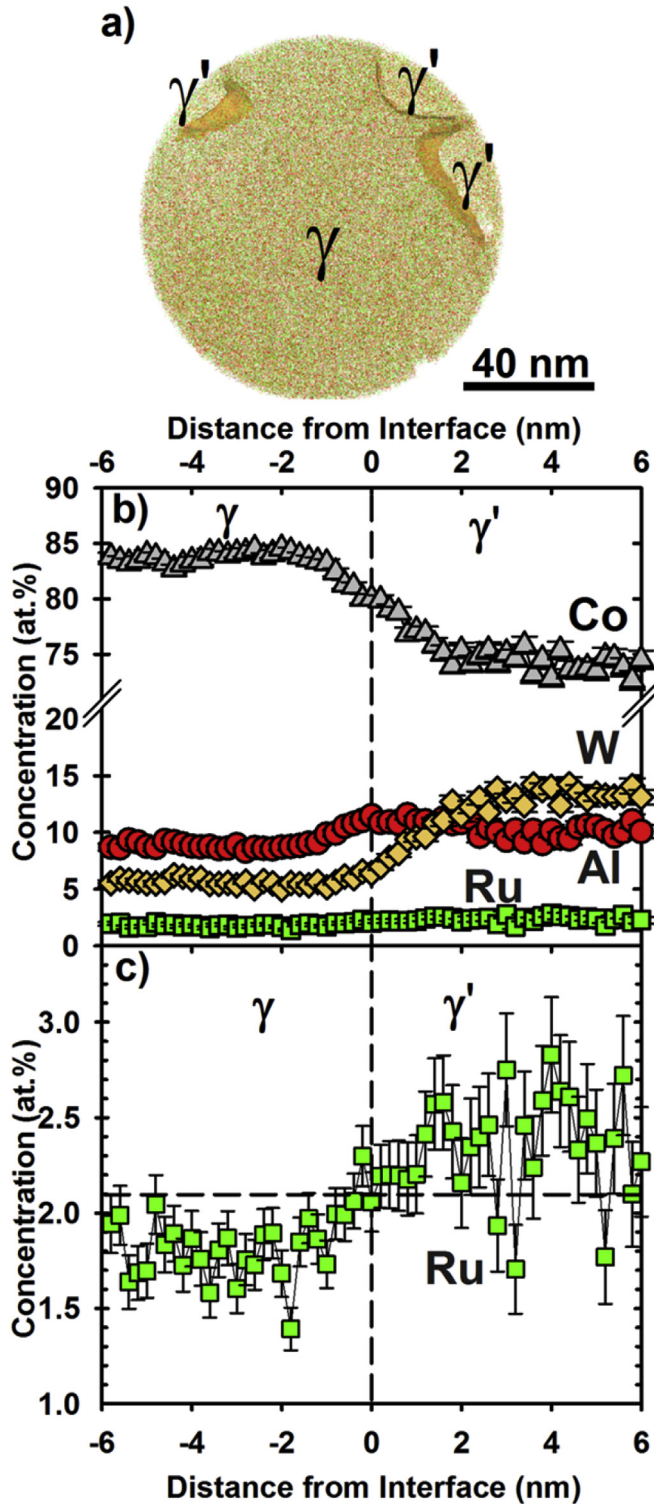


Fig. 7. Elemental γ/γ' partitioning of Co-9.4Al-7.5W-2.1Ru at.% after 16 h of aging at 900 °C: (a) top-view cross-section of APT reconstruction consisting of 9 million ions collected and containing three partial γ' precipitates described by 9 at.% W iso-concentration surface. (b) Proximity histogram, averaged among the three partial γ' precipitates, of constituent elements where the zero value (0) of the interface is defined as the inflection point of the majority species, Co. (c) Higher resolution portion of Ru proximity histogram. The dashed horizontal line represents the bulk Ru concentration of 2.1 at.%.

observed experimentally in multi-component Ni-base superalloys [16,19,20,23] as well as in Ni–Al–Ru and Ni–Al–Re–Ru alloys

[17,18,61], whose values of $K_{Ru}^{\gamma'/\gamma}$ are consistently below unity, in the range 0.2–0.6.

Our results demonstrate that Ru partitions to the γ' -phase in regions exhibiting a (γ plus γ') microstructure. The partitioning coefficients $K_X^{\gamma'/\gamma}$ for representative quaternary Co–Al–W–X alloys reported in the archival literature are displayed in Fig. 8 for comparison. The effect of Ru is obtained indirectly using our investigation of Ru partitioning, along with the experimental result [13] that the addition of 2 at. % Ru to a Co-8.9Al-9.8W alloy reduces the γ' -solvus temperature by 8 K; this result is in agreement with the observed trend that quaternary elemental additions that exhibit weak γ' -phase partitioning ($1 > K_X^{\gamma'/\gamma} > 2$) have a limited effect on the γ' solvus-temperature. This is in contrast to those elemental additions exhibiting strong partitioning to either γ (Cr, Fe, Mn), which decrease the γ' solvus-temperature by up to 20 K, or to γ' (Ti, Ta, Nb), which increase the γ' solvus-temperature by 50–80 K [3,7,10,13,62]. Tungsten also partitions to γ' -precipitates [13,15,59,63] and it has a positive effect on the γ' solvus-temperature of ternary Co–Al–W; Pyczak et al. [63] measured experimentally the γ' solvus-temperatures of Co-8.5Al-7.4W at.%, Co-8.5Al-8.7W at.%, and Co-8.9Al-10.3W at.%, reporting a decrease in γ' solvus-temperature of about 20 K per 1 at.% reduction of W [63]. This observation putatively suggests a γ' solvus-temperature of 1329 K for a Co-8.9Al-12W at.% alloy, which would be analogous to the series of Co-8.8-9.8-2X at.% alloys studied by Omori et al. [13]. The experimental value of the partitioning coefficient is strongly dependent on a number of factors, including alloy composition, the presence of additional alloying elements, aging time, and aging temperature. Qualitatively, experimental studies have demonstrated that Ti [3,7,10,13,62], Ta [3,7,10,13,60,62], Nb [3,13], V [13], Mo [13,60], W [13,15,59,63], Hf [7], Ir [62], Ni [3,13,15], and Ru (present study) partition to the γ' -phase, while Cr [3,13], Mn [13], and Fe [3,13] partition to the γ -phase in Co-based alloys. Less well-understood, but important for future studies, are synergistic effects among quaternary, quinary, and higher order alloying additions, because as many as 10 to 12 alloying elements may be necessary for a Co-based alloy that has long-term stability at very elevated temperatures.

A lever rule diagram [43], Fig. 9, was constructed using the bulk average composition, C_i^{bulk} , for every element i measured using EDS and the γ - and γ' -compositions (C_i^γ and $C_i^{\gamma'}$, respectively) measured utilizing APT for the 16 h aged sample. The γ' -volume-fraction, $\phi_{\gamma'}$, was determined by calculating the slope using a linear regression analysis, employing the mass-balance equation:

$$\phi_{\gamma'} = (C_i^{bulk} - C_i^\gamma) / (C_i^{\gamma'} - C_i^\gamma) \quad (6)$$

From Fig. 9, we determined a $\phi_{\gamma'}$ value of $24.8 \pm 1.8\%$, which agrees within experimental error with the value measured stereologically employing SEM micrographs ($25.41 \pm 0.04\%$), Fig. 3. This close agreement between the two characterization techniques lends credence to the veracity of our phase compositions reported using APT, with only three partial γ' -precipitates contained in the 3D reconstruction.

3.1.3. Discontinuous transformation at long aging times

After 128 h aging, the discontinuously transformed regions, initiating at grain boundaries, exhibit significant growth, Fig. 10. By 256 h aging, the formerly two-phase (γ plus γ') microstructure is >90% transformed. The discontinuous region consists of three phases, whose measured compositions are given in Table 1. These phases are identified as alternating lamellae of Co-rich γ (fcc)-matrix, Co_3W (taken to be $D0_{19}$) phase, as well as a blocky-phase CoAl (taken to have the B2 structure) phase, which is observed within the discontinuous region and along grain boundaries, Fig. 10.

Table 1
Compositions of observed phases in Co-9.4Al-7.5W-2.1Ru at.% alloy. All values are in at. %.

Region (aging time)	Phase(s)	Measurement method	Co	Al	W	Ru
γ plus γ' (16 h)	γ (f.c.c.)	APT	83.41 \pm 0.07	8.88 \pm 0.07	5.79 \pm 0.13	1.86 \pm 0.15
	γ'	APT	74.30 \pm 0.41	10.08 \pm 0.54	13.15 \pm 0.61	2.36 \pm 0.27
Discontinuously-transformed region (256 h)	γ (f.c.c.)	APT	85.20 \pm 0.21	8.44 \pm 0.14	5.20 \pm 0.12	1.15 \pm 0.05
	Co ₃ W (D0 ₁₉)	APT	74.91 \pm 0.39	1.82 \pm 0.12	21.57 \pm 0.27	1.69 \pm 0.09
	CoAl (B2)	EDS ^a	47	35	3	15

^a The error attributed to EDS measurements is taken to be ± 1 at. %.

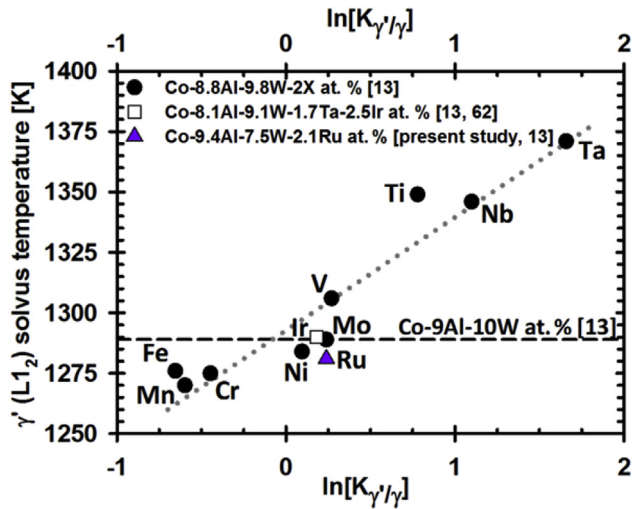


Fig. 8. Change in γ' -solvus of Co-9Al-10W-2X compared to Co-9Al-10W measured by differential scanning calorimetry (DSC) versus the natural log of the partitioning coefficient. The horizontal dashed black line denotes the solvus temperature of Co-9Al-10W at. % reported in Ref. [13]. Elements represented by solid black circles: $K_{\gamma'/\gamma}$ and the change in γ' -solvus were reported in Ref. [13]. $K_{\text{Ir}}^{\gamma'/\gamma}$ was reported by Ref. [62] incorporating DSC results from Ref. [13]. $K_{\text{Ru}}^{\gamma'/\gamma}$ is from the present study of Co-9.4Al-7.5W-2.1Ru, incorporating DSC results from Ref. [13] for Co-8.8Al-9.8W-2Ru at. %.

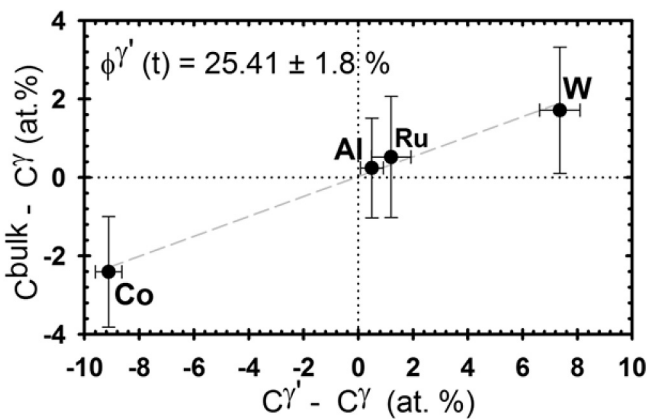


Fig. 9. Graphical representation of the lever rule (Eq. (6)); volume fraction calculated via APT composition measurements of γ - and γ' -phases and the composition of the bulk alloy measured via EDS. The error associated with the EDS measurements is assumed to be 1 at. %.

Phase identification is inferred from the measured compositions and the Co–Al–W phase diagram at 900 °C [1] and the Co–Al phase diagram [64], as well as morphological characteristics; for verification, the crystallographic structure will be confirmed experimentally by diffraction techniques. The γ -matrix composition measured by LEAP tomography, is nearly identical to that present in the γ/γ' region, Table 1. This suggests that the discontinuous

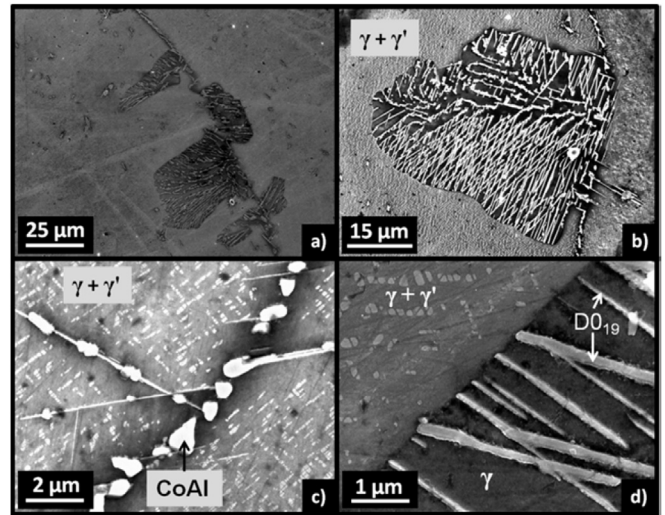


Fig. 10. Discontinuously-transformed microstructure at 128 h at 900 °C: (a) transformed colony spreading into bulk (γ plus γ') from the grain boundary; (b) transformed regions spreading outward from grain boundary (c) grain boundary containing Ru-rich CoAl-type precipitates. (d) close-up of interface between (γ plus γ') region and discontinuous lamellar region containing γ and D0₁₉ phases.

transformation reaction does not affect the mean γ -matrix composition, but rather the two other phases, D0₁₉ and B2, which are created solely by the decomposition of the γ' -precipitates. For the D0₁₉ needle-shaped precipitates, LEAP tomographic measurement, Fig. 11, indicate that Co comprises ~ 75 at.% of its composition, suggesting that the ~ 4 at.% of Al and Ru present in this phase are most likely involved in replacing W on its sublattice. The phase composition is then anticipated to be Co₃(W,Al, Ru). The B2 phase has a blocky morphology and is observed both along the GB and within the bulk discontinuously transformed region, usually in contact with D0₁₉ needle-like precipitates. The larger B2 precipitates are ~ 1 μm in diameter, which is sufficiently large to be investigated via SEM-EDS. The measured composition of this phase, Table 1, is 47Co-35Al-3W-15Ru at.%. It is probable that this phase is an off-stoichiometric version of CoAl(B2), based on similar observations and phase compositions in other Co-base systems; notably 49.2Co-29.5Al-1.9W-2.0Ta-17.5Ir at. % measured in a bulk Co-8.6Al-9.7W-1.0Ta-1.7Ir at. % alloy aged at 900 °C for 400 h [62], which compares favorably with our EDS measurements, Table 1. The intermetallic CoAl structure at 900 °C can contain a range of Co concentrations from 47 to 60 at.% Co, implying phases with the compositions Co₄₇(Al, Ru, W)₅₃ to Co₆₀(Al, Ru, W)₄₀. Additionally, because EDS detects x-rays generated not only from a sample's near surface region, but rather from the entire interaction volume (up to 1 μm^3). It is possible that some of the phase compositions measured utilizing EDS are due to a signal from the surrounding γ -matrix if a γ/CoAl interface exists within the subsurface interaction volume.

Turnbull [65] developed an approximate model for predicting the growth velocity of discontinuous lamellae, which he applied to

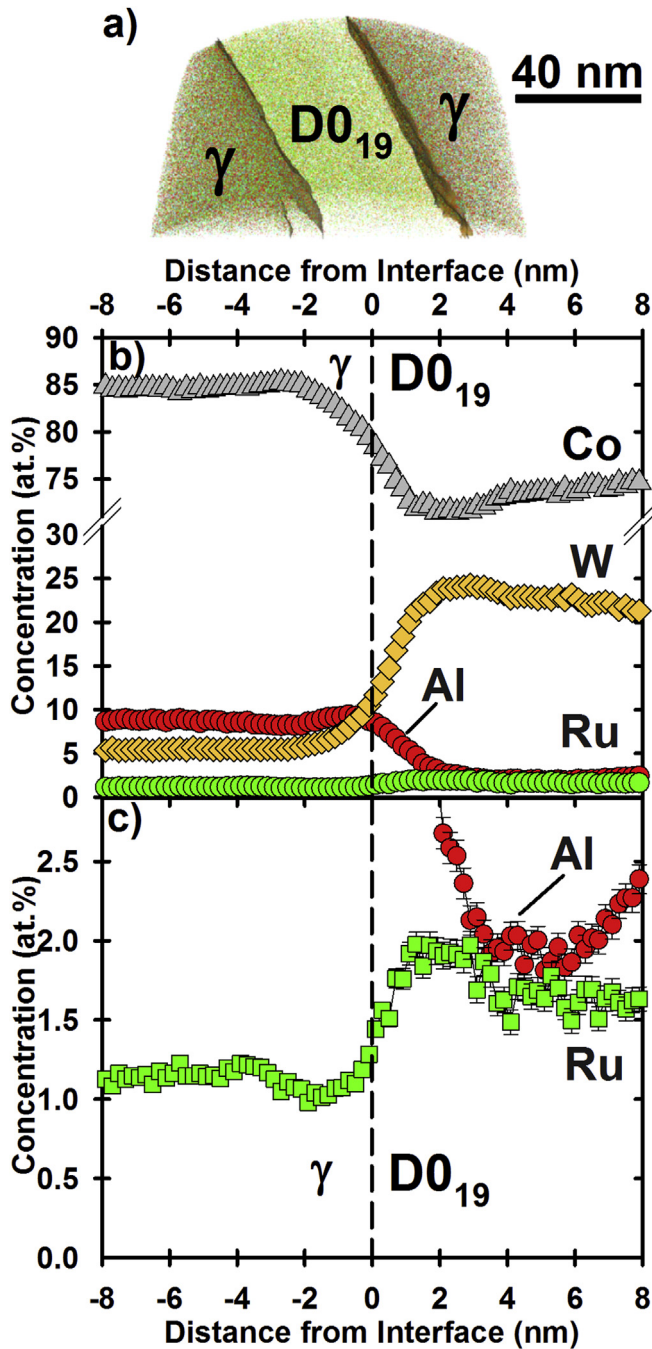


Fig. 11. Elemental partitioning of Co-9.4Al-7.5W-2.1Ru at.% after 256 h at 900 °C: (a) side-view of APT reconstruction consisting of 24 million ions collected and containing a lamellar portion of a single D0₁₉ precipitate bordered by γ . The heterophase boundary is described by a 20 at.% W iso-concentration surface. (b) Proximity histogram (averaged between the two interfaces) of constituent elements where the zero (0) interface is defined as the inflection point of the majority species, Co. (c) Magnified portion of the Ru proximity histogram.

a Co–Cr–Ti–Mo–V alloy exhibiting discontinuous growth of alternating bands of γ (f.c.c.) and Co₃Ti [66]. Applying the Turnbull model, the growth velocity, V , of discontinuous lamellae of γ - and D0₁₉ phases is given by:

$$v = \left(\frac{C_0^i - C_E^i}{C_0} \right) \frac{D_B \delta}{S^2}; \quad (7)$$

Where C_0^i is the bulk concentration of solute species i , C_E^i is the concentration of solute i in the γ -lamellar, D_B is the diffusivity along the heterophase interface between lamellae, δ is the thickness of this interfacial region ~ 1 nm, and S is the interlamellar spacing within the discontinuous region. Taking V as the constant growth velocity of discontinuous lamellae traversing the average maximum distance between the cell and the heterophase interface as measured from SEM micrographs, 32 ± 14 μm , during 128 h at 900 °C. Substituting our value for W , the dominant solute species in the transformed D0₁₉ lamellae, taking $C_0^W = 7.5$ at.%, $C_E^W = 5.8$ at.%, and $S = 0.92$ μm , we obtain a value of 2×10^{-22} $\text{m}^3 \text{s}^{-1}$ for the diffusivity of W times the value of δ along the heterophase interface, $D_B \delta$. The archival literature values for grain boundary diffusivity in Co alloys are sparse; $D_B \delta$ of W in a Co-5at.% W alloy at 800 °C and pure Co at 700 °C are 6×10^{-20} and 2×10^{-23} $\text{m}^3 \text{s}^{-1}$, respectively [67]. Note the value obtained from our calculation is a bulk average, whereas the extent of the discontinuous transformation varies from cell-to-cell and grain-to-grain. Nevertheless, our value of 2×10^{-22} $\text{m}^3 \text{s}^{-1}$ at 900 °C is with an order of magnitude of the diffusivity along grain boundaries in a Co alloy: 6×10^{-20} $\text{m}^3 \text{s}^{-1}$ for a Co-5at.% W alloy at 800 °C, and 2×10^{-23} $\text{m}^3 \text{s}^{-1}$ for pure Co at 700 °C [67], suggesting that W diffusion along heterophase interfaces may be a source of the observed rapid microstructural transformation occurring in this alloy.

The average composition over several 100×100 μm regions on the surface of the bulk cross-section was measured using EDS for the specimen aged 168 h at 900 °C. The average composition of the (γ plus γ') containing regions is 81.4Co-8.6Al-7.8W-2.2Ru at.%, compared to 80.5Co-9.4Al-7.9W-2.2Ru at.% for discontinuously-transformed regions and to the composition of the material in the as-solutionized state, 81.0Co-9.4Al-7.5W-2.1Ru at.%; these measurements are within error, taken to be ± 1 at.%, for our EDS measurements. The rapid kinetics of the transformation between 128 and 256 h of aging indicates that the three-phase discontinuously transformed region is more thermodynamically stable than the two-phase (γ plus γ') microstructure for the alloy composition investigated. One possibility is that the addition of Ru results in a bulk composition that is no longer within the very small (γ plus γ') phase-field reported in the Co–Al–W ternary system [1] and that adjusting the balance of the W and Al concentrations in the alloy results in a more stable γ' -phase. Furthermore, alloying with strong γ' forming-elements, such as Ti or Ta, is necessary to obtain a stable γ plus γ' microstructure.

4. Conclusions

The microstructural evolution of a quaternary Co-9.4Al-7.5W-2.1Ru at.% model superalloy aged at 900 °C was investigated and compared to a ternary base alloy with the composition Co-8.8Al-7.3W at.%. SEM was utilized to determine the mean radius and volume fractions of the γ' (L1₂)-precipitates and to assess the stability of the two-phase (γ plus γ') microstructure. LEAP tomography was employed to determine the partitioning behavior of the constitutive elements between the (f.c.c) γ -matrix and the γ' (L1₂)-precipitates. The following conclusions are reached:

- Ruthenium partitions slightly to the γ' (L1₂) -phase in Co-9.4Al-7.5W-2.1Ru at.%, with a partitioning coefficient $K_{\text{Ru}}^{\gamma'/\gamma} = 1.27 \pm 0.18$, after 16 h aging at 900 °C, displaying the opposite tendency to that observed in Ni-base superalloys and predicted by a first-principles calculation at 0 K for Co–Al– \oplus W–Ru [30].

- Co, Al, and W exhibit similar partitioning behaviors in the investigated Co–Al–W–Ru alloy to those observed in the archival literature for other model Co-base systems:

$$(K_{W}^{\gamma/\gamma'} = 2.27 \pm 0.15), (K_{Co}^{\gamma/\gamma'} = 0.89 \pm 0.01), \text{ and } (K_{Al}^{\gamma/\gamma'} = 1.13 \pm 0.07).$$

- Regions of (γ plus γ') persist for 256 h at 900 °C in the Co–Al–W–Ru alloy, permitting the measurement of γ' -precipitate radii, Fig. 4, and volume fraction, Fig. 3, as a function of aging time. Ruthenium additions do not affect significantly the volume fraction or coarsening kinetics of the γ' (L1₂)-phase when compared to the base Co–Al–W ternary alloy.
- A discontinuous transformation of the (γ plus γ') microstructure is observed after 128 h of aging at 900 °C in the Ru-containing alloy. The transformed three-phase region nucleates at γ -grain-boundaries, which consumes the two-phase (γ plus γ') region. It contains the same γ (f.c.c.) Co-rich solid-solution (Co-8.44Al-5.20W-1.15Ru at.%), needle-like precipitates with the D0₁₉ structure (Co-1.82Al-21.57W-1.69Ru at.%) and blocky precipitates with the B2 structure (Co-35Al-3W-15Ru at.%). Only (γ plus γ') phase regions are observed, utilizing SEM, for the ternary Co–Al–W alloy aged for 1024 h at 900 °C.

Acknowledgements

This work was performed with financial assistance from award 70NANB14H012 from the U.S. Department of Commerce, National Institute of Standards and Technology, as part of the Center for Hierarchical Materials Design (CHiMaD) at Northwestern University. The LEAP tomograph at NUAPT was purchased and upgraded with funding from NSF-MRI (DMR-0420532) and ONR-DURIP (N00014-0400798, N00014-0610539, N00014-0910781) grants. Instrumentation at NUAPT was also supported by the Initiative for Sustainability and Energy at Northwestern (ISEN). This work also made use of the shared facilities at the Materials Research Center of Northwestern University (DMR-1121262). We also thank gratefully Dr. Ronald D. Noebe (NASA Glenn Research Center) for casting the base ternary alloy, Prof. Peter W. Voorhees and Dr. John Thompson (Northwestern University) for providing us with simulated precipitate radius distributions, so-called PSDs, for the Akaiwa-Voorhees model, and Mr. Robert Schuld (NU) for assistance with the preparation and heat treatment of the ternary alloy.

References

- [1] J. Sato, T. Omori, K. Oikawa, I. Ohnuma, R. Kainuma, K. Ishida, Cobalt-base high-temperature alloys, *Science* 312 (2006) 90–91.
- [2] R.C. Reed, *The Superalloys Fundamentals and Applications*, Cambridge University Press, 2006.
- [3] M. Ooshima, K. Tanaka, N.L. Okamoto, K. Kishida, H. Inui, Effects of quaternary alloying elements on the γ' solvus temperature of Co–Al–W based alloys with fcc/L1₂ two-phase microstructures, *J. Alloys Compd.* 508 (2010) 71–78.
- [4] A. Suzuki, G.C. DeNolf, T.M. Pollock, Flow stress anomalies in γ/γ' two-phase Co–Al–W-base alloys, *Scr. Mater.* 56 (2007) 385–388.
- [5] J.E. Saal, C. Wolverton, Thermodynamic stability of Co–Al–W L1₂ γ' , *Acta Mater.* 61 (2013) 2330–2338.
- [6] S. Kobayashi, Y. Tsukamoto, T. Takasugi, H. Chinen, T. Omori, K. Ishida, S. Zaeferrer, Determination of phase equilibria in the Co-rich Co–Al–W ternary system with a diffusion-couple technique, *Intermetallics* 17 (2009) 1085–1089.
- [7] S. Kobayashi, Y. Tsukamoto, T. Takasugi, The effects of alloying elements (Ta, Hf) on the thermodynamic stability of γ' -Co₃(Al,W) phase, *Intermetallics* 31 (2012) 94–98.
- [8] F. Xue, H.J. Zhou, X.F. Ding, M.L. Wang, Q. Feng, Improved high temperature γ' stability of Co–Al–W-base alloys containing Ti and Ta, *Mater. Lett.* 112 (2013) 215–218.
- [9] C.H. Zenk, S. Neumeier, H.J. Stone, M. Göken, Mechanical properties and lattice misfit of γ/γ' strengthened Co-base superalloys in the Co–W–Al–Ti quaternary system, *Intermetallics* 55 (2014) 28–39.
- [10] I. Povstugar, P.-P. Choi, S. Neumeier, A. Bauer, C.H. Zenk, M. Göken, D. Raabe, Elemental partitioning and mechanical properties of Ti- and Ta-containing Co–Al–W-base superalloys studied by atom probe tomography and nano-indentation, *Acta Mater.* 78 (2014) 78–85.
- [11] T.M. Pollock, J. Dibbern, M. Tsunekane, J. Zhu, A. Suzuki, New Co-based gamma-gamma prime high-temperature alloys, *J. Mater.* 62 (2010) 58–63.
- [12] A. Bauer, S. Neumeier, F. Pyczak, M. Göken, Microstructure and creep strength of different γ/γ' -strengthened Co-base superalloy variants, *Scr. Mater.* 63 (2010) 1197–1200.
- [13] T. Omori, K. Oikawa, J. Sato, I. Ohnuma, U.R. Kattner, R. Kainuma, K. Ishida, Partition behavior of alloying elements and phase transformation temperatures in Co–Al–W-base quaternary systems, *Intermetallics* 32 (2013) 274–283.
- [14] K. Shinagawa, T. Omori, J. Sato, K. Oikawa, I. Ohnuma, R. Kainuma, K. Ishida, Phase equilibria and microstructure on γ' phase in Co–Ni–Al–W system, *Mater. Trans.* 49 (2008) 1474–1479.
- [15] S. Meher, H.Y. Yan, S. Nag, D. Dye, R. Banerjee, Solute partitioning and site preference in γ/γ' cobalt-base alloys, *Scr. Mater.* 67 (2012) 850–853.
- [16] S. Tin, A.C. Yeh, A.P. Ofori, R.C. Reed, S.S. Babu, M.K. Miller, Atomic partitioning of Ruthenium in Ni-based superalloys, in: K.A. Green, T.M. Pollock, H. Harada (Eds.), *Superalloys 2004*: TMS, 2004, pp. 735–741.
- [17] Y. Zhou, D. Isheim, G. Hsieh, R.D. Noebe, D.N. Seidman, Effects of ruthenium on phase separation in a model Ni–Al–Cr–Ru superalloy, *Philos. Mag.* 93 (2013) 1326–1350.
- [18] Y. Zhou, Z. Mao, C. Booth-Morrison, D.N. Seidman, The partitioning and site preference of ruthenium or ruthenium in model nickel-based superalloys: an atom-probe tomographic and first-principles study, *Appl. Phys. Lett.* 93 (2008) 171905.
- [19] L.J. Carroll, Q. Feng, J.F. Mansfield, T.M. Pollock, Elemental partitioning in Ru-containing nickel-base single crystal superalloys, *Mater. Sci. Eng. A* 457 (2007) 292–299.
- [20] L.J. Carroll, Q. Feng, J.F. Mansfield, T.M. Pollock, High refractory, low misfit Ru-containing single-crystal superalloys, *Metall. Mater. Trans. A* 37 (2006) 2927–2938.
- [21] S. Neumeier, F. Pyczak, M. Göken, The influence of ruthenium and rhenium on the local properties of the γ - and γ' -phase in nickel-base superalloys and their consequences for alloy behavior, in: R.C. Reed, K.A. Green, P. Caron, T.P. Gabb, M.G. Fahrman, E.S. Huron, S.A. Woodard (Eds.), *Superalloys 2008*: TMS (The Minerals, Metals & Materials Society), 2008, pp. 109–119.
- [22] R.C. Reed, A.C. Yeh, S. Tin, S.S. Babu, M.K. Miller, Identification of the partitioning characteristics of ruthenium in single crystal superalloys using atom probe tomography, *Scr. Mater.* 51 (2004) 327–331.
- [23] J.S. Van Sluytman, A.L. Fontaine, J.M. Cairney, T.M. Pollock, Elemental partitioning of platinum group metal containing Ni-base superalloys using electron microprobe analysis and atom probe tomography, *Acta Mater.* 58 (2010) 1952–1962.
- [24] A. Volek, F. Pyczak, R.F. Singer, H. Mughrabi, Partitioning of Re between γ and γ' phase in nickel-base superalloys, *Scr. Mater.* 52 (2005) 141–145.
- [25] L.L. Zhu, H.Y. Qi, L. Jiang, Z.P. Jin, J.C. Zhao, Experimental determination of the Ni–Cr–Ru phase diagram and thermodynamic reassessments of the Cr–Ru and Ni–Cr–Ru systems, *Intermetallics* 64 (2015) 86–95.
- [26] F. Sun, J.X. Zhang, Influence of Ru on the microstructure of Ni-Base single crystal superalloys, *Adv. Mater.* Res. 306–307 (2011) 562–571.
- [27] A. Sato, H. Harada, T. Yokokawa, T. Murakumo, Y. Koizumi, T. Kobayashi, H. Imai, The effects of ruthenium on the phase stability of fourth generation Ni-base single crystal superalloys, *Scr. Mater.* 54 (2006) 1679–1684.
- [28] K. Matuszewski, R. Rettig, H. Matysiak, Z. Peng, I. Povstugar, P. Choi, J. Müller, D. Raabe, E. Spiecker, K.J. Kurzydowski, R.F. Singer, Effect of ruthenium on the precipitation of topologically close packed phases in Ni-based superalloys of 3rd and 4th generation, *Acta Mater.* 95 (2015) 274–283.
- [29] M. Chen, C.-Y. Wang, First-principles investigation of the site preference and alloying effect of Mo, Ta and platinum group metals in γ' -Co₃(Al,W), *Scr. Mater.* 60 (2009) 659–662.
- [30] M. Chen, C.-Y. Wang, First-principles study of the partitioning and site preference of Re or Ru in Co-based superalloys with interface, *Phys. Lett. A* 374 (2010) 3238–3242.
- [31] S. Kobayashi, Y. Tsukamoto, T. Takasugi, Phase equilibria in the Co-rich Co–Al–W–Ti quaternary system, *Intermetallics* 19 (2011) 1908–1912.
- [32] J.C. Russ, R.T. Dehoff, *Practical Stereology*, second ed., Plenum Press, New York, NY.
- [33] D.N. Seidman, Three-dimensional atom-probe tomography: advances and applications, *Annu. Rev. Mater. Res.* 37 (2007) 127–158.
- [34] B.W. Krakauer, J.G. Hu, S.M. Kuo, R.L. Mallick, A. Seki, D.N. Seidman, J.P. Baker, R.J. Loyd, A system for systematically preparing atom-probe field-ion-microscope specimens for the study of internal interfaces, *Rev. Sci. Instrum.* 61 (1990) 3390.
- [35] O.C. Hellman, J.A. Vandenbroucke, J. Rüsing, D. Isheim, D.N. Seidman, Analysis of three-dimensional atom-probe data by the proximity histogram, *Microsc. Microanal.* 6 (2000) 437–444.
- [36] O.C. Hellman, D.N. Seidman, Measurement of the Gibbsian interfacial excess of solute at an interface of arbitrary geometry using three-dimensional atom probe microscopy, *Mater. Sci. Eng. A* (2002) 24–28.
- [37] M.K. Miller, R.G. Forbes, *Atom-probe Tomography: the Local Electrode Atom Probe*, Springer, New York, 2014.
- [38] M.K. Miller, E.A. Kenik, Atom probe tomography: a technique for nanoscale characterization, *Microsc. Microanal.* 10 (2004) 336–341.
- [39] C.K. Sudbrack, T.D. Ziebell, R.D. Noebe, D.N. Seidman, Effects of a tungsten

- addition on the morphological evolution, spatial correlations and temporal evolution of a model Ni–Al–Cr superalloy, *Acta Mater.* 56 (2008) 448–463.
- [40] A. Hazotte, J. Lacaze, Chemically oriented g' plate development in a nickel base superalloy, *Scr. Metall.* 23 (1989) 1877–1882.
- [41] R.A. MacKay, M.V. Nathal, g' coarsening in high volume fraction nickel-base alloys, *Acta Metall. Mater.* 38 (1990) 993–1005.
- [42] B. Hinze, J. Rösler, F. Schmitz, Production of nanoporous superalloy membranes by load-free coarsening of γ' -precipitates, *Acta Mater.* 59 (2011) 3049–3060.
- [43] Y. Amouyal, D.N. Seidman, An atom-probe tomographic study of freckle formation in a nickel-based superalloy, *Acta Mater.* 59 (2011) 6729–6742.
- [44] Y. Amouyal, D.N. Seidman, The role of hafnium in the formation of misoriented defects in Ni-based superalloys: an atom-probe tomographic study, *Acta Mater.* 59 (2011) 3321–3333.
- [45] Q. Feng, L.J. Carroll, T.M. Pollock, Solidification segregation in ruthenium-containing nickel-base superalloys, *Metall. Mater. Trans. A* 37 (2006) 1949–1962.
- [46] B. Hinze, J. Rösler, Advanced fabrication of nanoporous Ni-based superalloy membranes, *Procedia Mater. Sci.* 4 (2014) 46–50.
- [47] A. Epishin, T. Link, U. Brukner, B. Fedelich, P. Portella, Effects of segregation in Nickel-base superalloys: dendritic stresses, in: K.A. Green, T.M. Pollock, H. Harada (Eds.), *Superalloys 2004: TMS, 2004*, pp. p.537–543.
- [48] H.-Y. Yan, V.A. Vorontsov, D. Dye, Alloying effects in polycrystalline γ' strengthened Co–Al–W base alloys, *Intermetallics* 48 (2013) 44–53.
- [49] A. Bauer, S. Neumeier, F. Pyczak, R.F. Singer, M. Göken, Creep properties of different γ' -strengthened Co-base superalloys, *Mater. Sci. Eng. A* 550 (2012) 333–341.
- [50] E.Y. Plotnikov, Z. Mao, R.D. Noebe, D.N. Seidman, Temporal evolution of the $\gamma(\text{fcc})/\gamma'(L1_2)$ interfacial width in binary Ni–Al alloys, *Scr. Mater.* 70 (2014) 51–54.
- [51] C.J. Kuehmann, P.W. Voorhees, Ostwald ripening in ternary alloys, *Metall. Mater. Trans. A* 27A (1996) 937–943.
- [52] T. Philippe, P.W. Voorhees, Ostwald ripening in multicomponent alloys, *Acta Mater.* 61 (2013) 4237–4244.
- [53] A.J. Ardell, The effect of volume fraction on particle coarsening: theoretical considerations, *Acta Metall.* 20 (1972) 61–71.
- [54] S. Neumeier, H.U. Rehman, J. Neuner, C.H. Zenk, S. Michel, S. Schuwalow, J. Rogal, R. Drautz, M. Göken, Diffusion of solutes in fcc Cobalt investigated by diffusion couples and first principles kinetic Monte Carlo, *Acta Mater.* 106 (2016) 304–312.
- [55] Z. Mao, C. Booth-Morrison, C.K. Sudbrack, G. Martin, D.N. Seidman, Kinetic pathways for phase separation: an atomic-scale study in Ni–Al–Cr alloys, *Acta Mater.* 60 (2012) 1871–1888.
- [56] E.Y. Plotnikov, M. Yildirim, S.-I. Baik, Z. Mao, Y. Li, D. Cecchetti, R. Noebe, G. Martin, D. Seidman, A Correlative Four-dimensional Study of Phase Separation at the Subnanoscale to Nanoscale of a Ni–Al Alloy, 2016 submitted for publication.
- [57] A.D. Brailsford, P. Wynblatt, The dependence of ostwald ripening kinetics on particle volume fraction, *Acta Metall.* 27 (1978) 489–497.
- [58] N. Akaiwa, P.W. Voorhees, Late-stage phase separation: dynamics, spatial correlations, and structure functions, *Phys. Rev. E* 49 (1994) 3860–3880.
- [59] P.J. Bocchini, E.A. Lass, K.-W. Moon, M.E. Williams, C.E. Campbell, U.R. Kattner, D.C. Dunand, D.N. Seidman, Atom-probe tomographic study of γ/γ' interfaces and compositions in an aged Co–Al–W superalloy, *Scr. Mater.* 68 (2013) 563–566.
- [60] S. Meher, R. Banerjee, Partitioning and site occupancy of Ta and Mo in Co-base γ/γ' alloys studied by atom probe tomography, *Intermetallics* 49 (2014) 138–142.
- [61] Y. Zhou, Phase Separation on a Subnanoscale in Model Ni–Al–Cr-based Superalloys, *Materials Science and Engineering*, vol. PhD, Northwestern University, Evanston, IL, 2010.
- [62] A. Bauer, S. Neumeier, F. Pyczak, M. Göken, Influence of iridium on the properties of γ' -strengthened Co-Base superalloys, *Adv. Eng. Mater.* 17 (2015) 748–754.
- [63] F. Pyczak, A. Bauer, M. Göken, U. Lorenz, S. Neumeier, M. Oehring, J. Paul, N. Schell, A. Schreyer, A. Stark, F. Symanzik, The effect of tungsten content on the properties of $L1_2$ -hardened Co–Al–W alloys, *J. Alloys Compd.* 632 (2015) 110–115.
- [64] A.J. McAlister, Al–Co (Aluminum–Cobalt), in: second ed., in: T.B. Massalski (Ed.), *Binary Phase Diagrams*, 1, 1990, pp. 136–138.
- [65] D. Turnbull, Theory of cellular precipitation, *Acta Metall.* 3 (1955) 55–63.
- [66] A. Bhowmik, S. Neumeier, S. Rhode, H.J. Stone, Allotropic transformation induced stacking faults and discontinuous coarsening in a γ - γ' Co-base alloy, *Intermetallics* 59 (2015) 95–101.
- [67] I. Kaur, W. Gust, Data for grain and interphase boundary diffusion, *Diffus. Solid Metals Alloys* 26 (1990) 657–668.